Supporting information：

Significant seasonal variations in isotopic composition of atmospheric total gaseous mercury at forest sites in China caused by vegetation and mercury sources

Xuewu Fu[*,†,‡], Hui Zhang[†,§], Chen Liu[†,§], Hui Zhang[†], Che-Jen Lin[ǀ], Xinbin Feng[*,†,‡,§]

[†]State Key Laboratory of Environmental Geochemistry, Institute of Geochemistry, Chinese Academy of Sciences, Guiyang, 550081, China,

[‡]CAS Center for Excellence in Quaternary Science and Global Change, Xi'an, 710061, China,

[§]University of Chinese Academy of Sciences, Beijing, 100049, China

[ǀ]Center for Advances in Water and Air Quality, Lamar University, Beaumont, TX, USA

Number of pages: 21
Number of Tables: 4
Number of figures: 13

Text S1: Analysis of cumulative NDVI (∑NDVI), cumulative anthropogenic Hg^0 emission (∑Hg^0 emission), cumulative wildfire (∑fire), and fractional air mass residence time (ARTs)

In this study, means of cumulative NDVI (∑NDVI), cumulative anthropogenic Hg^0 emission (∑Hg^0 emission), cumulative wildfire (∑fire), and fractional air mass residence time (ARTs) of each of the TGM isotope sample were calculated. To do this, the origin and atmospheric transport of air masses of each of the sample were firstly determined by calculating the 48-h backward trajectories of air masses ended at the sampling sites (at a height of 100 m above ground) every 4 h using the TrajStat Geographical Information System based software and gridded meteorological data (Global Data Assimilation System, GDAS1) from the U.S. National Oceanic and Atmospheric Administration (NOAA) [*Wang et al.*, 2009]. The duration of trajectories was selected to investigate the exposure of air masses to local and regional vegetation activity (represented by the satellite-based normalized difference vegetation index, NDVI), primary anthropogenic GEM emissions, wildfire, and oceans that may have influenced the TGM isotopic compositions in MCB.

Mean ∑NDVI: The mean ∑NDVI of each TGM isotope sample was calculated by averaging the global gridded NDVI values (from the National Aeronautic and Space Administration Earth Observation platform at 16 days temporal and 0.1° spatial resolution) encountered by the air masses during the preceding two days of atmospheric transport regardless of transport height, which is calculated using eq (1):

$$Mean\,\sum NDVI_{(N)} = \frac{\sum_{l=1}^{L}\sum_{(i=1,j=1)}^{(i=n,j=m)} NDVI_{ij} \times \tau_{ijl}}{L} \qquad (1)$$

where mean $\sum NDVI_{(N)}$ is the mean NDVI encountered by the 2-day backward air masses during the whole sampling period of the TGM isotope sample (N), $NDVI_{ij}$ is the NDVI value (dimensionless) in a grid cell (ij) during the sampling period of TGM isotope sample (N), τ_{ijl} is the number of trajectory segment endpoints in grid cell (i, j) for backward trajectory l divided by the total number of endpoints of the same trajectory l, n is number of grid cells in longitude in the study domain covering the origin and transporting pathway of backward trajectory l, m is number of grid cells in latitude in the study domain covering the origin and transporting pathway of backward trajectory l, and L is the total number of backward trajectories calculated for the TGM isotope sample (N).

Mean ∑Hg^0 emission: The mean ∑Hg^0 emission of each TGM isotope sample was calculated by averaging the global gridded Hg^0 emissions in 2010 (from the Arctic Monitoring and Assessment programme (AMAP) at 0.5° spatial resolution, and the AMAP 2010 global gridded Hg^0 inventory is the most updated inventory released to the public) encountered by the air masses during the preceding two days of atmospheric transport regardless of transport height, which is calculated using eq (2):

$$Mean\,\sum Hg^0\ emission_{(N)} = \frac{\sum_{l=1}^{L}\sum_{(i=1,j=1)}^{(i=n,j=m)} {Hg^0}_{ij} \times \tau_{ijl}}{L} \qquad (2)$$

where mean $\sum Hg^0$ emission$_{(N)}$ is the mean Hg^0 emission encountered by the 2-day backward air masses during the whole sampling period of the TGM isotope sample (N), ${Hg^0}_{ij}$ is the Hg^0 emission (in kg/0.5 grid) in a grid cell (ij) in 2010, τ_{ijl} is the number of trajectory segment endpoints in grid cell (i, j) for backward trajectory l divided by the total number of endpoints of the same trajectory l, n is number of grid cells in longitude in the study domain covering the origin and transporting pathway of backward trajectory l, m is number of grid cells in latitude in the study domain covering the origin and transporting pathway of backward trajectory l, and L is the total number of backward trajectories calculated for the TGM isotope sample (N).

mean ∑fire: The mean ∑fire of each TGM isotope sample was calculated by averaging the global gridded actively burning fires (from the National Aeronautic and Space Administration Earth Observation platform at 8 days temporal and 0.1° spatial resolution) encountered by the air masses during the preceding two days of atmospheric transport regardless of transport height, which is calculated using eq (3):

$$Mean \sum Fire_{(N)} = \frac{\sum_{l=1}^{L} \sum_{(i=1,\, j=1)}^{(i=n,\, j=m)} Fire_{ij} \times \tau_{ijl}}{L} \qquad (3)$$

where mean $\sum Fire_{(N)}$ is the mean actively burning fires encountered by the 2-day backward air masses during the whole sampling period of the TGM isotope sample (N), $Fire_{ij}$ is the actively burning fires index (in fire pixels/1000km^2/day) in a grid cell (ij) during the sampling period of TGM isotope sample (N), τ_{ijl} is the number of trajectory segment endpoints in grid cell (i, j) for backward trajectory l divided by the total number of endpoints of the same trajectory l, n is number of grid cells in longitude in the study domain covering the origin and transporting pathway of backward trajectory l, m is number of grid cells in latitude in the study domain covering the origin and transporting pathway of backward trajectory l, and L is the total number of backward trajectories calculated for the TGM isotope sample (N).

Mean fractional oceanic ARTs: The mean fractional oceanic atmospheric residence times (ARTs) of each TGM isotope sample was the mean percentage of ARTs over ocean relative to the total ARTs, which is calculated using eq (4):

$$Mean\ fractional\ oceanic\ ARTs_{(N)} = \frac{\sum_{l=1}^{L} \sum \tau_{ocean}}{L} \qquad (4)$$

where mean fractional oceanic ARTs(N) is the mean percentage of ARTs over ocean relative to the total ARTs during the whole sampling period of TGM isotope sample (N), τ_{ocean} is the number of trajectory segment endpoints over ocean for backward trajectory l divided by the total number of endpoints of the same trajectory l, and L is the total number of backward trajectories calculated for the TGM isotope sample (N).

Table S1 Sample information, atmospheric TGM concentrations measured by CLC traps, atmospheric TGM isotopic compositions and associated analytical uncertainties (2σ) at the sites under (1 m a.g.l.) and above (25 m a.g.l.) forest canopy in Mt. Changbai (MCB) forest in northeastern China and at the site under forest canopy in Mt. Ailao forest (MAL) in southwestern China.

Location	Classification	Sampling period	TGM conc. ($ng\ m^{-3}$)	$\delta^{199}Hg$ (‰)	$\delta^{200}Hg$ ‰	$\delta^{201}Hg$ ‰	$\delta^{202}Hg$ ‰	$\Delta^{199}Hg$ ‰	$\Delta^{200}Hg$ ‰	$\Delta^{201}Hg$ ‰	$\delta^{199}Hg$ 2σ (‰)	$\delta^{200}Hg$ 2σ (‰)	$\delta^{201}Hg$ 2σ (‰)	$\delta^{202}Hg$ 2σ (‰)	$\Delta^{199}Hg$ 2σ (‰)	$\Delta^{200}Hg$ 2σ (‰)	$\Delta^{201}Hg$ 2σ (‰)
Mt. Changbai	Under canopy	2015/4/10-2015/4/20	1.63	-0.11	0.12	0.08	0.31	-0.19	-0.04	-0.15	0.07	0.13	0.14	0.12	0.06	0.11	0.09
	Above canopy		1.53	-0.10	0.04	-0.01	0.26	-0.16	-0.09	-0.20	0.09	0.14	0.26	0.17	0.06	0.11	0.14
Mt. Changbai	Under canopy	2015/4/20-2015/4/30	1.67	-0.11	0.04	-0.02	0.22	-0.16	-0.07	-0.18	0.10	0.14	0.14	0.17	0.06	0.11	0.09
	Above canopy		1.62	-0.15	-0.03	-0.13	0.37	-0.24	-0.21	-0.41	0.07	0.13	0.16	0.12	0.06	0.11	0.12
Mt. Changbai	Under canopy	2015/4/30-2015/5/10	1.54	-0.08	0.14	0.09	0.42	-0.19	-0.07	-0.22	0.10	0.13	0.26	0.17	0.14	0.17	0.39
	Above canopy		1.55	-0.17	0.00	-0.10	0.15	-0.20	-0.08	-0.22	0.07	0.13	0.14	0.12	0.06	0.11	0.09
Mt. Changbai	Under canopy	2015/5/10-2015/5/25	1.56	-0.07	0.16	0.14	0.42	-0.18	-0.05	-0.18	0.07	0.13	0.14	0.12	0.06	0.11	0.09
	Above canopy		1.62	-0.14	0.07	0.04	0.29	-0.21	-0.07	-0.18	0.07	0.13	0.14	0.12	0.06	0.11	0.09
Mt. Changbai	Under canopy	2015/5/25-2015/6/5	1.62	-0.14	0.07	0.13	0.33	-0.23	-0.10	-0.12	0.07	0.13	0.14	0.12	0.06	0.11	0.09
	Above canopy		1.75	-0.18	-0.04	-0.12	0.12	-0.21	-0.11	-0.21	0.07	0.13	0.14	0.12	0.06	0.11	0.09
Mt. Changbai	Under canopy	2015/6/5-2015/6/16	1.42	0.16	0.53	0.63	1.09	-0.11	-0.01	-0.19	0.08	0.13	0.14	0.12	0.06	0.11	0.09
	Above canopy		1.44	0.10	0.41	0.55	0.86	-0.12	-0.03	-0.10	0.07	0.13	0.14	0.12	0.06	0.11	0.09
Mt. Changbai	Under canopy	2015/6/16-2015/6/26	--	--	--	--	--	--	--	--	--	--	--	--	--	--	--
	Above canopy		1.52	0.10	0.34	0.52	0.78	-0.09	-0.05	-0.07	0.07	0.13	0.14	0.19	0.06	0.11	0.09
Mt. Changbai	Under canopy	2015/6/26-2015/7/6	1.27	0.21	0.63	0.92	1.33	-0.13	-0.04	-0.09	0.08	0.13	0.17	0.12	0.06	0.11	0.10
	Above canopy		1.32	0.06	0.35	0.45	0.94	-0.17	-0.12	-0.26	0.10	0.13	0.26	0.17	0.14	0.17	0.39
Mt. Changbai	Under canopy	2015/7/6-2015/7/17	1.36	0.16	0.52	0.76	1.15	-0.13	-0.06	-0.11	0.07	0.13	0.20	0.15	0.06	0.11	0.09
	Above canopy		1.48	0.02	0.31	0.41	0.68	-0.15	-0.03	-0.10	0.08	0.13	0.14	0.12	0.07	0.11	0.09
Mt. Changbai	Under canopy	2015/7/17-2015/7/28	1.36	0.19	0.57	0.80	1.24	-0.12	-0.05	-0.13	0.08	0.13	0.17	0.12	0.06	0.11	0.10
	Above canopy		1.50	0.06	0.31	0.43	0.79	-0.13	-0.08	-0.16	0.10	0.13	0.20	0.14	0.06	0.11	0.09

Mt. Changbai	Under canopy	2015/7/28-2015/8/8	1.24	0.25	0.69	0.96	1.48	-0.13	-0.05	-0.15	0.09	0.14	0.26	0.17	0.06	0.11	0.14
	Above canopy		1.44	0.13	0.46	0.64	1.06	-0.14	-0.07	-0.15	0.07	0.13	0.14	0.12	0.06	0.11	0.09
Mt. Changbai	Under canopy	2015/8/8-2015/8/19	1.21	0.29	0.72	1.05	1.45	-0.07	-0.01	-0.04	0.13	0.15	0.23	0.18	0.08	0.11	0.10
	Above canopy		1.39	0.17	0.50	0.72	1.04	-0.09	-0.03	-0.06	0.07	0.13	0.14	0.12	0.06	0.11	0.09
Mt. Changbai	Under canopy	2015/8/19-2015/8/30	0.87	0.25	0.69	0.97	1.42	-0.11	-0.03	-0.09	0.08	0.13	0.14	0.12	0.06	0.11	0.09
	Above canopy		1.06	0.19	0.58	0.84	1.24	-0.13	-0.04	-0.09	0.13	0.15	0.23	0.18	0.08	0.11	0.10
Mt. Changbai	Under canopy	2015/8/30-2015/9/12	0.95	0.27	0.75	1.14	1.64	-0.14	-0.07	-0.09	0.13	0.15	0.23	0.18	0.08	0.11	0.10
	Above canopy		1.12	0.13	0.57	0.88	1.42	-0.23	-0.15	-0.19	0.11	0.14	0.23	0.14	0.08	0.11	0.12
Mt. Changbai	Under canopy	2015/9/12-2015/9/22	1.10	0.01	0.37	0.55	0.86	-0.20	-0.06	-0.10	0.08	0.13	0.14	0.12	0.07	0.11	0.09
	Above canopy		1.18	-0.09	0.22	0.22	0.61	-0.24	-0.08	-0.24	0.07	0.13	0.14	0.12	0.06	0.11	0.09
Mt. Changbai	Under canopy	2015/9/22-2015/10/3	1.54	-0.02	0.30	0.36	0.76	-0.22	-0.09	-0.21	0.10	0.13	0.20	0.14	0.06	0.11	0.09
	Above canopy		1.55	-0.07	0.23	0.24	0.61	-0.22	-0.07	-0.22	0.07	0.13	0.20	0.15	0.06	0.11	0.09
Mt. Changbai	Under canopy	2015/10/3-2015/10/13	1.24	-0.06	0.18	0.17	0.39	-0.16	-0.01	-0.13	0.07	0.13	0.14	0.12	0.06	0.11	0.09
	Above canopy		1.28	-0.03	0.18	0.24	0.49	-0.15	-0.07	-0.13	0.07	0.13	0.14	0.12	0.06	0.11	0.09
Mt. Changbai	Under canopy	2015/10/13-2015/10/23	--	--	--	--	--	--	--	--	--	--	--	--	--	--	--
	Above canopy		1.33	-0.11	0.08	0.01	0.23	-0.16	-0.03	-0.16	0.07	0.13	0.14	0.12	0.06	0.11	0.09
Mt. Changbai	Under canopy	2015/10/23-2015/11/4	1.29	-0.09	0.16	0.16	0.41	-0.19	-0.04	-0.15	0.07	0.13	0.14	0.12	0.06	0.11	0.09
	Above canopy		1.23	-0.13	0.16	0.10	0.41	-0.23	-0.04	-0.21	0.07	0.13	0.14	0.12	0.06	0.11	0.09
Mt. Changbai	Under canopy	2015/11/4-2015/11/18	1.51	-0.05	0.12	0.14	0.28	-0.12	-0.02	-0.07	0.07	0.13	0.14	0.12	0.06	0.11	0.09
	Above canopy		1.52	-0.03	0.19	0.21	0.49	-0.16	-0.05	-0.16	0.07	0.13	0.14	0.12	0.06	0.11	0.09
Mt. Changbai	Under canopy	2015/11/18-2015/11/28	1.67	-0.07	0.14	0.15	0.40	-0.17	-0.07	-0.15	0.07	0.13	0.14	0.18	0.06	0.11	0.09
	Above canopy		1.63	-0.12	0.07	0.07	0.31	-0.19	-0.08	-0.16	0.07	0.13	0.14	0.12	0.06	0.11	0.09
Mt. Changbai	Under canopy	2015/11/28-2015/12/10	1.70	-0.08	0.17	0.13	0.43	-0.19	-0.04	-0.19	0.07	0.13	0.14	0.12	0.06	0.11	0.09
	Above canopy		1.81	-0.18	0.00	0.06	0.24	-0.24	-0.12	-0.12	0.07	0.13	0.14	0.12	0.06	0.11	0.09
Mt. Changbai	Under canopy	2015/12/10-2015/12/22	1.73	-0.10	0.11	0.01	0.23	-0.16	-0.01	-0.16	0.07	0.13	0.14	0.12	0.06	0.11	0.09
	Above canopy		1.72	-0.10	0.08	0.00	0.21	-0.16	-0.03	-0.16	0.07	0.13	0.14	0.12	0.07	0.11	0.14

Mt. Changbai	Under canopy	2015/12/22-2016/1/23	1.85	-0.16	0.10	0.04	0.33	-0.25	-0.07	-0.21	0.07	0.13	0.14	0.12	0.06	0.11	0.09
	Above canopy		1.74	-0.12	0.16	0.17	0.42	-0.22	-0.05	-0.15	0.10	0.13	0.20	0.12	0.08	0.11	0.13
Mt. Changbai	Under canopy	2016/1/23-2016/2/4	1.44	-0.13	0.12	0.08	0.37	-0.22	-0.06	-0.19	0.10	0.13	0.14	0.12	0.10	0.11	0.09
	Above canopy		1.45	-0.09	0.13	0.14	0.31	-0.17	-0.02	-0.09	0.07	0.13	0.14	0.12	0.06	0.11	0.09
Mt. Changbai	Under canopy	2016/2/4-2016/2/18	1.54	-0.09	0.13	0.12	0.30	-0.16	-0.02	-0.10	0.07	0.13	0.14	0.12	0.06	0.11	0.09
	Above canopy		1.49	-0.14	0.02	0.01	0.18	-0.19	-0.08	-0.13	0.07	0.13	0.14	0.12	0.06	0.11	0.09
Mt. Changbai	Under canopy	2016/2/18-2016/2/28	1.40	-0.10	0.08	0.07	0.24	-0.16	-0.04	-0.11	0.07	0.13	0.14	0.12	0.07	0.11	0.14
	Above canopy		1.38	-0.09	0.15	0.15	0.41	-0.19	-0.06	-0.15	0.07	0.13	0.14	0.12	0.07	0.11	0.14
Mt. Changbai	Under canopy	2016/2/28-2016/3/10	1.60	-0.17	0.12	0.05	0.32	-0.25	-0.04	-0.19	0.07	0.13	0.14	0.12	0.06	0.11	0.09
	Above canopy		1.57	-0.04	0.21	0.29	0.49	-0.16	-0.04	-0.08	0.07	0.13	0.14	0.12	0.07	0.11	0.09
Mt. Changbai	Under canopy	2016/3/10-2016/3/21	1.58	-0.12	0.09	0.01	0.30	-0.19	-0.06	-0.21	0.10	0.13	0.20	0.12	0.08	0.11	0.13
	Above canopy		1.57	-0.07	0.11	0.05	0.26	-0.14	-0.02	-0.14	0.07	0.13	0.14	0.12	0.06	0.11	0.09
Mt. Changbai	Under canopy	2016/3/21-2016/3/31	1.58	-0.15	-0.01	-0.09	0.12	-0.19	-0.08	-0.18	0.10	0.13	0.14	0.12	0.10	0.11	0.09
	Above canopy		--	--	--	--	--	--	--	--	--	--	--	--	--	--	--
Mt. Changbai	Under canopy	2016/331-2016/4/10	1.37	-0.07	0.17	0.21	0.44	-0.18	-0.05	-0.12	0.07	0.13	0.14	0.12	0.06	0.11	0.09
	Above canopy		--	--	--	--	--	--	--	--	--	--	--	--	--	--	--
Mt. Ailao	Under canopy	2017/1/1-2017/1/11	1.25	0.00	0.26	0.38	0.67	-0.17	-0.07	-0.12	0.07	0.13	0.14	0.12	0.06	0.11	0.09
Mt. Ailao	Under canopy	2017/1/11-2017/1/22	1.26	0.14	0.32	0.48	0.63	-0.02	0.00	0.00	0.07	0.13	0.14	0.12	0.06	0.11	0.09
Mt. Ailao	Under canopy	2017/1/12-2017/2/10	1.21	-0.04	-0.01	0.08	0.21	-0.10	-0.11	-0.08	0.07	0.13	0.14	0.12	0.06	0.11	0.09
Mt. Ailao	Under canopy	2017/2/10-2017/2/27	1.54	-0.03	0.09	0.16	0.29	-0.10	-0.06	-0.05	0.07	0.13	0.14	0.12	0.06	0.11	0.09
Mt. Ailao	Under canopy	2017/2/27-2017/3/15	1.68	-0.05	0.13	0.15	0.58	-0.20	-0.16	-0.29	0.07	0.13	0.14	0.12	0.06	0.11	0.09
Mt. Ailao	Under canopy	2017/3/15-2017/3/30	1.90	-0.09	0.03	0.02	0.19	-0.14	-0.07	-0.12	0.07	0.13	0.14	0.12	0.06	0.11	0.09
Mt. Ailao	Under canopy	2017/3/30-2017/4/27	2.40	-0.07	0.09	0.01	0.14	-0.10	0.02	-0.09	0.07	0.13	0.14	0.12	0.06	0.11	0.09
Mt. Ailao	Under canopy	2017/4/27-2017/5/13	2.81	0.04	0.00	-0.01	-0.10	0.07	0.05	0.06	0.07	0.13	0.14	0.12	0.06	0.11	0.09
Mt. Ailao	Under canopy	2017/5/13-2017/5/24	2.46	-0.07	0.07	0.12	0.25	-0.13	-0.06	-0.06	0.07	0.13	0.14	0.12	0.06	0.11	0.09

Mt. Ailao	Under canopy	2017/5/24-2017/6/13	1.98	-0.05	0.04	0.00	0.16	-0.09	-0.04	-0.12	0.07	0.13	0.14	0.12	0.06	0.11	0.09
Mt. Ailao	Under canopy	2017/7/18-2017/7/29	1.62	-0.17	-0.11	-0.22	-0.12	-0.14	-0.05	-0.13	0.07	0.13	0.14	0.12	0.06	0.11	0.09
Mt. Ailao	Under canopy	2017/7/29-2017/8/20	1.68	-0.12	-0.06	-0.19	-0.05	-0.10	-0.04	-0.16	0.07	0.13	0.14	0.12	0.06	0.11	0.09
Mt. Ailao	Under canopy	2017/8/30-2017/9/15	1.53	-0.11	0.00	-0.07	0.05	-0.13	-0.03	-0.11	0.07	0.13	0.14	0.12	0.06	0.11	0.09
Mt. Ailao	Under canopy	2017/9/15-2017/9/30	1.43	0.11	0.12	-0.05	0.08	0.09	0.08	-0.11	0.07	0.13	0.14	0.12	0.08	0.11	0.09
Mt. Ailao	Under canopy	2017/9/30-2017/10/16	1.49	-0.14	0.01	-0.09	0.07	-0.16	-0.03	-0.14	0.07	0.13	0.14	0.12	0.08	0.11	0.09
Mt. Ailao	Under canopy	2017/10/16-2017/10/29	1.58	-0.11	-0.13	-0.39	-0.20	-0.06	-0.03	-0.24	0.11	0.18	0.30	0.16	0.07	0.11	0.18
Mt. Ailao	Under canopy	2017/10/29-2017/11/14	1.75	-0.02	0.01	-0.03	0.04	-0.03	-0.01	-0.06	0.11	0.18	0.30	0.16	0.07	0.11	0.18
Mt. Ailao	Under canopy	2017/11/14-2017/11/30	1.45	0.18	0.23	0.44	0.39	0.08	0.03	0.15	0.07	0.13	0.14	0.12	0.06	0.11	0.09
Mt. Ailao	Under canopy	2017/11/30-2017/12/15	1.14	0.01	0.30	0.36	0.62	-0.14	-0.01	-0.10	0.07	0.13	0.14	0.12	0.07	0.11	0.09
Mt. Ailao	Under canopy	2017/12/15-2017/12/27	1.63	-0.07	0.04	0.04	0.18	-0.12	-0.06	-0.10	0.07	0.13	0.14	0.12	0.06	0.11	0.09
Mt. Ailao	Under canopy	2017/12/27-2018/1/17	1.53	-0.04	0.01	0.07	0.21	-0.09	-0.09	-0.09	0.07	0.13	0.14	0.12	0.06	0.11	0.09
Mt. Ailao	Under canopy	2018/1/17-2018/1/30	1.78	0.09	0.23	0.33	0.43	-0.02	0.01	0.01	0.07	0.13	0.14	0.12	0.06	0.11	0.09
Mt. Ailao	Under canopy	2018/1/30-2018/2/13	1.98	0.03	0.17	0.21	0.32	-0.05	0.01	-0.03	0.07	0.13	0.14	0.12	0.06	0.11	0.09

Table S2 Average Hg isotopic compositions of international standard NIST SRM 3177, lichen CRM (BCR 482), and standard addition of NIST 3133 to CLC traps over analytical sessions in this study. The 2σ represent the 2 times of the standard error (2 sd) of the mean isotopic compositions measured over analytical sessions.

Standard type	n	Recovery (%)		δ^{199}Hg (‰)		δ^{200}Hg (‰)		δ^{201}Hg (‰)		δ^{202}Hg (‰)		Δ^{199}Hg (‰)		Δ^{200}Hg (‰)		Δ^{201}Hg (‰)	
		Mean	1σ	‰	2σ	‰	2σ	‰	2σ	‰	2σ	‰	2σ	‰	2σ	‰	2σ
NIST SRM 3177	22	--	--	-0.15	0.06	-0.28	0.07	-0.42	0.08	-0.53	0.09	-0.02	0.06	-0.01	0.05	-0.03	0.07
Lichen CRM (BCR 482)	6	94.2	4.1	-1.02	0.06	-0.72	0.09	-1.84	0.13	-1.61	0.19	-0.62	0.05	0.08	0.06	-0.63	0.14
Standard addition of NIST SRM 3133 to CLC traps	10	92.3	4.6	0.00	0.07	-0.03	0.13	-0.02	0.14	-0.02	0.12	0.01	0.06	-0.03	0.11	0.00	0.09

Table S3 Statistical summary of the seasonal means of TGM concentrations, $\delta^{202}Hg_{TGM}$, $\Delta^{199}Hg_{TGM}$, $\Delta^{200}Hg_{TGM}$ values, local NDVI, as well as seasonal means of cumulative exposure of air masses to NDVI (∑NDVI), anthropogenic Hg^0 emissions (∑Hg^0 emission), wildfire (∑Fire), fractional oceanic ARTs, and meteorological parameters (Air Temperature, solar radiation, air relative humidity, and wind speed) during the preceding 2 days in the present study. The four seasons are defined following the meteorological definition in the Northern Hemisphere, with spring runs from March to May, summer runs from Jun to August, autumn runs from September to November, and winter runs from December to February.

Site	Season	n	TGM conc. (ng m^{-3})	$\delta^{202}Hg_{TGM}$ (‰)	$\Delta^{199}Hg_{TGM}$ (‰)	$\Delta^{200}Hg_{TGM}$ (‰)	Local mean NDVI	Mean ∑NDVI	Mean ∑Hg^0 emission (kg/0.5 grid/h)	Mean ∑Fire (Pixels/1000 km^2/day/h)	Mean fractional oceanic ARTs	Air temperature (°C)	Solar radiation (w m^{-2})	Relative humidity (%)	Wind speed (m s^{-1})
MCB-under forest canopy	Spring	9	1.57	0.32	-0.20	-0.06	0.43	0.33	70.8	0.36	0.13				
	Summer	7	1.25	1.31	-0.11	-0.04	0.85	0.82	55.6	0.12	0.20				
	Autumn	7	1.32	0.68	-0.17	-0.05	0.49	0.46	57.8	0.20	0.05				
	Winter	6	1.61	0.32	-0.19	-0.04	0.18	0.11	78.8	0.11	0.05				
	All year	**29**	**1.44**	**0.66**	**-0.17**	**-0.05**	**0.49**	**0.43**	**65.8**	**0.20**	**0.11**				
MCB-above forest canopy	Spring	7	1.60	0.28	-0.19	-0.09	0.43	0.33	70.8	0.36	0.13	7.0	256	54.7	1.8
	Summer	8	1.39	0.92	-0.13	-0.06	0.85	0.82	55.6	0.12	0.20	18.3	268	83.1	0.8
	Autumn	8	1.36	0.57	-0.20	-0.07	0.49	0.46	57.8	0.20	0.05	5.1	195	72.8	1.1
	Winter	6	1.60	0.30	-0.19	-0.06	0.18	0.11	78.8	0.11	0.05	-12.0	99	68.7	1.3
	All year	**29**	**1.48**	**0.52**	**-0.18**	**-0.07**	**0.49**	**0.43**	**65.8**	**0.20**	**0.11**	**4.6**	**204**	**69.9**	**1.2**
MAL-under forest canopy	Spring	4	2.25	0.21	-0.10	-0.04	0.63	0.63	48.8	0.23	0.01	11.3	195	--	3.5
	Summer	3	1.76	0.00	-0.11	-0.04	0.77	0.77	67.4	0.11	0.00	15.4	198	--	2.7
	Autumn	6	1.54	0.07	-0.03	0.00	0.76	0.78	83.8	0.10	0.00	12.7	142	--	3.2
	Winter	9	1.48	0.40	-0.09	-0.04	0.71	0.71	33.7	0.13	0.01	7.5	166	--	4.0
	All year	**22**	**1.70**	**0.17**	**-0.08**	**-0.03**	**0.72**	**0.72**	**58.4**	**0.14**	**0.00**	**11.8**	**165**	**--**	**3.3**

Table S4 Statistical summary of the seasonal means of $\delta^{202}Hg_{TGM}$, $\Delta^{199}Hg_{TGM}$ and cumulative exposure of air masses to anthropogenic Hg^0 emissions (∑Hg^0 emission) during the preceding 2 days at Pic du Midi in France and urban sites in China. $\delta^{202}Hg_{TGM}$ and $\Delta^{199}Hg_{TGM}$ values were from previous studies [*Fu et al.*, 2016; *Yu et al.*, 2016; *Xu et al.*, 2017]. Seasonal means of ∑Hg^0 emission at these sites are calculated using the method described in Section 2.4 of this study.

Site	Type	Time period	Season	$\delta^{202}Hg_{TGM}$ (mean ± 1σ, ‰)	$\Delta^{199}Hg_{TGM}$ (mean ± 1σ, ‰)	Mean ∑Hg^0 emission (kg/0.5 grid/h)
Pic du Midi, France	High-altitude	2012.02 - 2013.01	Spring	0.09 ± 0.09	-0.19 ± 0.03	8.1
			Summer	0.09 ± 0.06	-0.21 ± 0.02	7.8
			Autumn	0.20 ± 0.04	-0.23 ± 0.03	7.9
			Winter	0.36 ± 0.10	-0.20 ± 0.03	6.2
Beijing, China	Urban	2013.06 – 2014.12	Spring	-1.29 ± 1.05	-0.01 ± 0.04	376
			Summer	-0.53 ± 0.42	-0.03 ± 0.09	508
			Autumn	-0.36 ± 0.38	-0.05 ± 0.10	511
			Winter	-1.00 ± 0.41	-0.02 ± 0.02	239
Ningbo, China	Urban	2014.01- 2014.12	Spring	-0.27 ± 0.26	-0.08 ± 0.04	302
			Summer	-0.35 ± 0.24	-0.07 ± 0.06	313
			Autumn	-0.13 ± 0.44	-0.09 ± 0.07	331
			Winter	-0.00 ± 019	-0.11 ± 0.02	356
Xi’an, China	Urban	2011.10 - 2012.10	Spring	0.13 ± 0.61	0.01 ± 0.03	174
			Summer	−0.18 ± 0.13	−0.01 ± 0.03	200
			Autumn	−0.27 ± 0.23	−0.01 ± 0.03	192
			Winter	−0.07 ± 0.46	0.00 ± 0.06	136
Guiyang, China	Urban	2012.05 - 2013.10	Spring	-0.43 ± 0.16	0.03 ± 0.04	148
			Summer	-0.73 ± 0.30	0.03 ± 0.06	123
			Autumn	-0.61 ± 0.18	0.05 ± 0.06	145
			Winter	-0.52 ± 0.20	0.06 ± 0.03	137

Figure S1 Locations of the forest sampling sites in this study and the gridded (0.1° × 0.1°) variations of the satellite-based normalized difference vegetation index (NDVI) between July 2015 and January 2016 in East Asia (NDVIJul - NDVIJan).

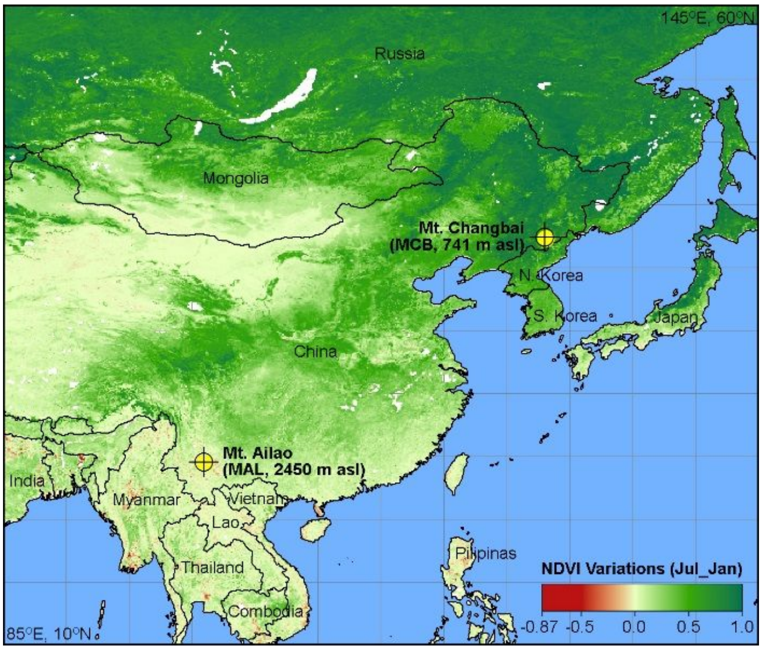

Figure S2 Schematic diagram of the cold vapor phase separator

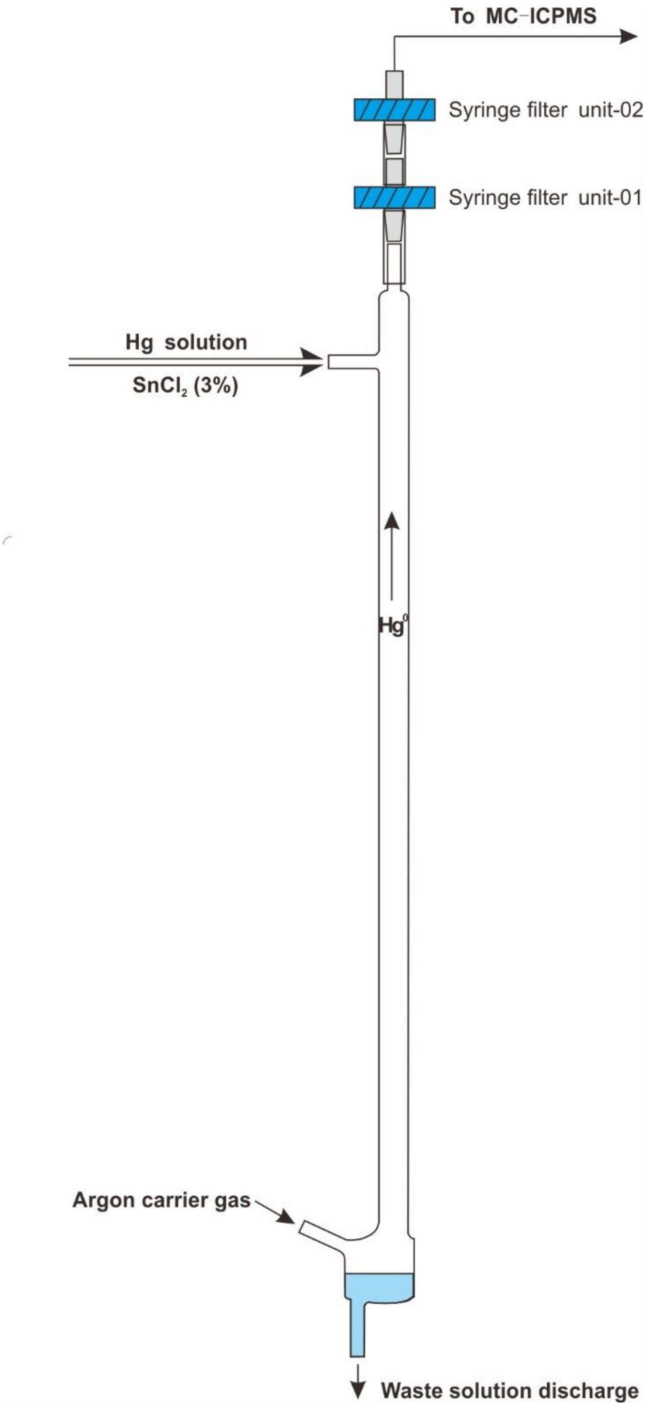

Figure S3 Temporal variations in local mean NDVI and mean cumulative exposure of air masses to NDVI during the preceding 2 days (mean ∑NDVI) in MCB and MAL forests during the studied periods of TGM isotopic composition in this study.

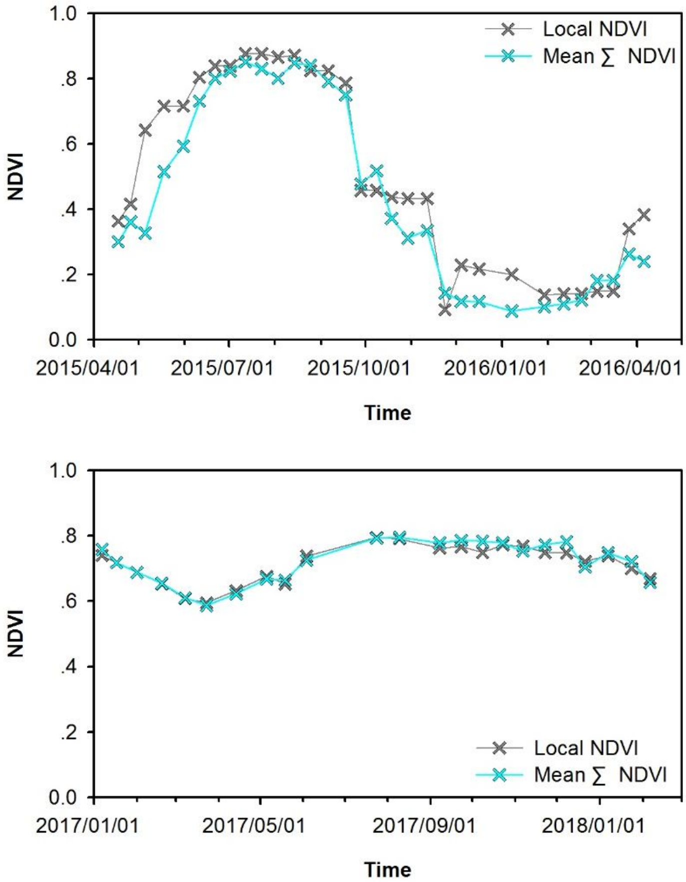

Figure S4 Comparisons of ∑NDVI, ∑Hg^0 emission, ∑fire, and fractional oceanic ARTs between the preceding 2 days and 1 day and 5 days in MCB forest. The methods for calculations of ∑NDVI, ∑Hg^0 emission, ∑fire, and fractional oceanic ARTs are shown in Section 2.4 in the present study. Backward trajectories were all ended at a height of 100 m above ground level in MCB.

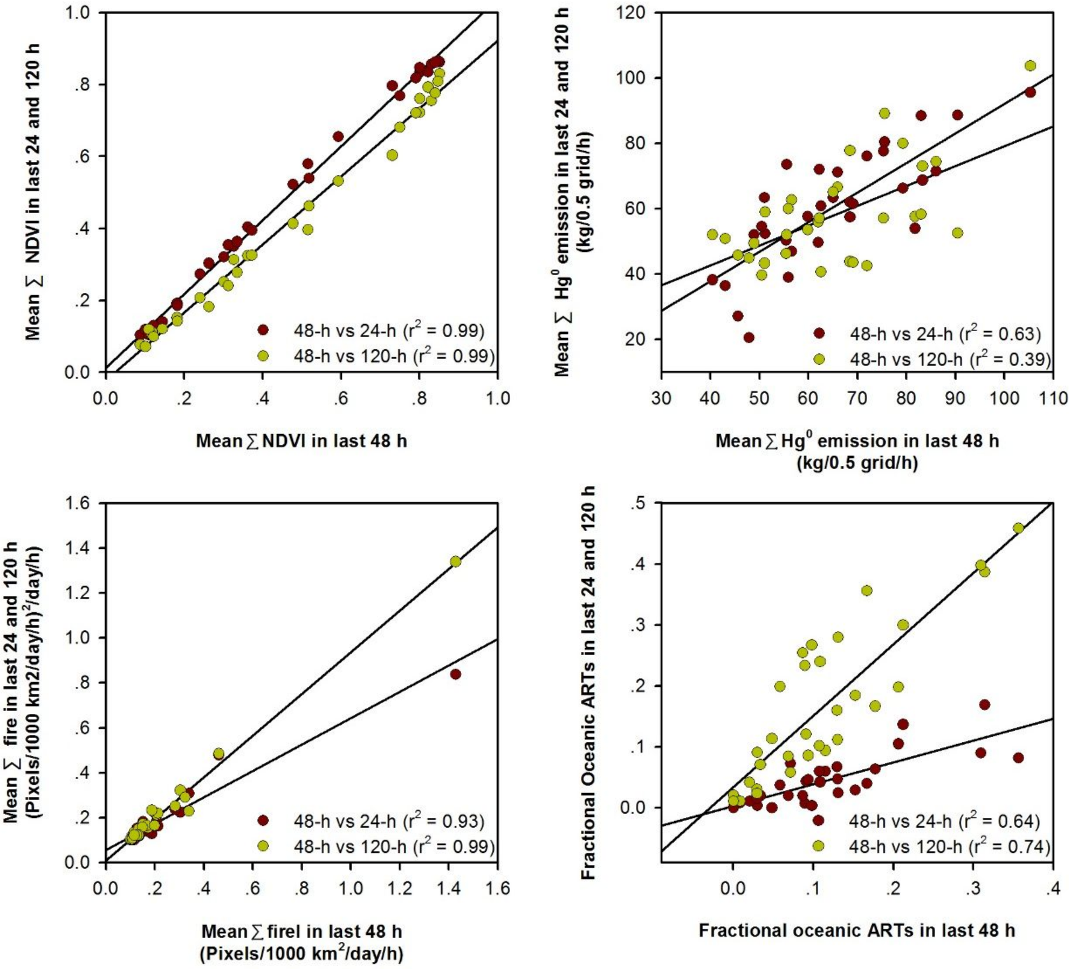

Figure S5 Comparisons of ∑NDVI, ∑Hg^0 emission, ∑fire, and fractional oceanic ARTs between the preceding 2 days and 1 day and 5 days in MAL forest. The methods for calculations of ∑NDVI, ∑Hg^0 emission, ∑fire, and fractional oceanic ARTs are shown in Section 2.4 in the present study. Backward trajectories were all ended at a height of 100 m above ground level in MAL.

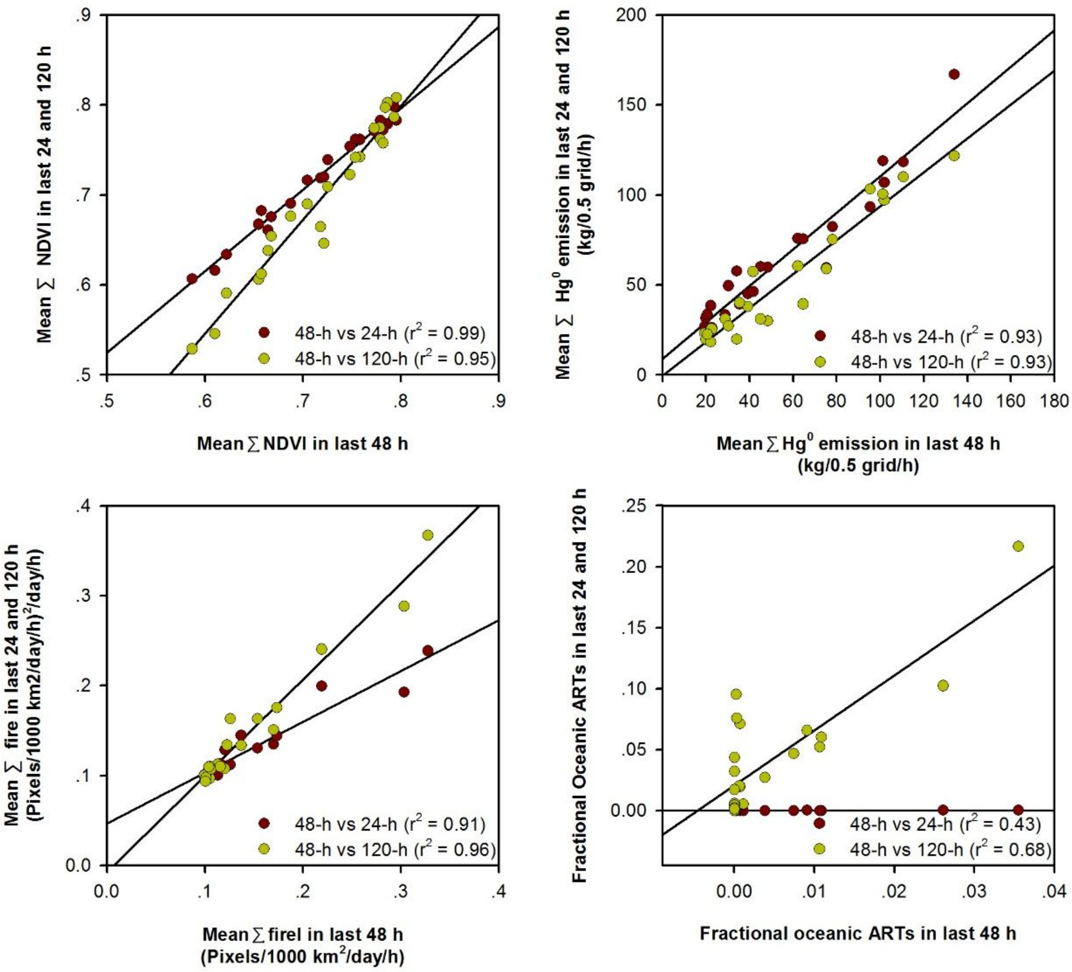

Figure S6 Temporal variations in vertical gradient in atmospheric TGM $\Delta^{199}Hg$ values (Δ-$\Delta^{199}Hg_{TGM}$ =$\Delta^{199}Hg_{TGM-1m}$ -$\Delta^{199}Hg_{TGM-25m}$) and TGM $\Delta^{200}Hg$ values (Δ-$\Delta^{200}Hg_{TGM}$ =$\Delta^{200}Hg_{TGM-1m}$ –$\Delta^{200}Hg_{TGM-25m}$) in the MCB forest.

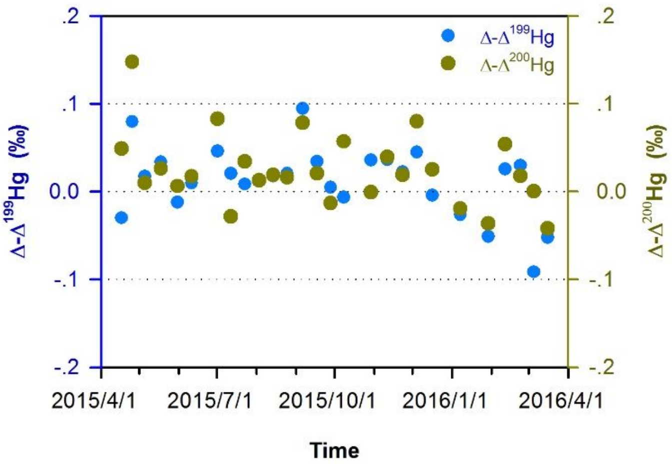

Figure S7 Vertical gradient in TGM δ^{202}Hg (Δ-δ^{202}Hg) versus the net fraction of TGM remaining after penetrating the forest canopy (Fraction of TGM (f_R)) in MCB forest during the study period. The Rayleigh fraction model is based on the MDF fractionation factor of -2.89‰ between atmospheric TGM pool and vegetation observed by Demers et al. [2013].

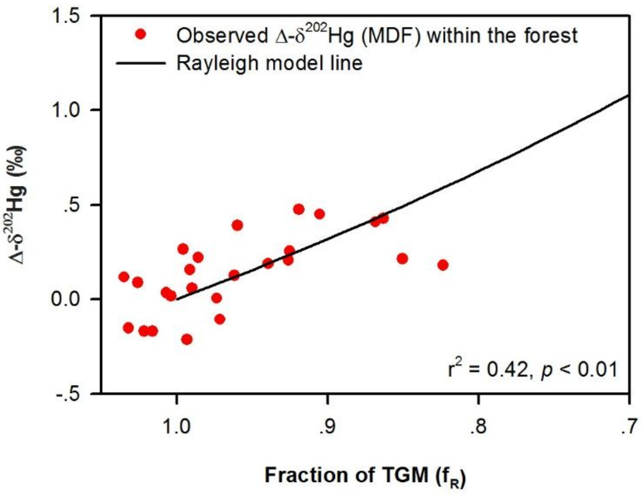

Figure S8 Seasonal variations in atmospheric TGM $\Delta^{200}Hg$ at sites of (A) under forest canopy (1 m a.s.l) in Mt. Changbai, (B) above forest canopy (25 m a.s.l) in Mt. Changbai, and (C) under forest canopy in Mt. Ailao.

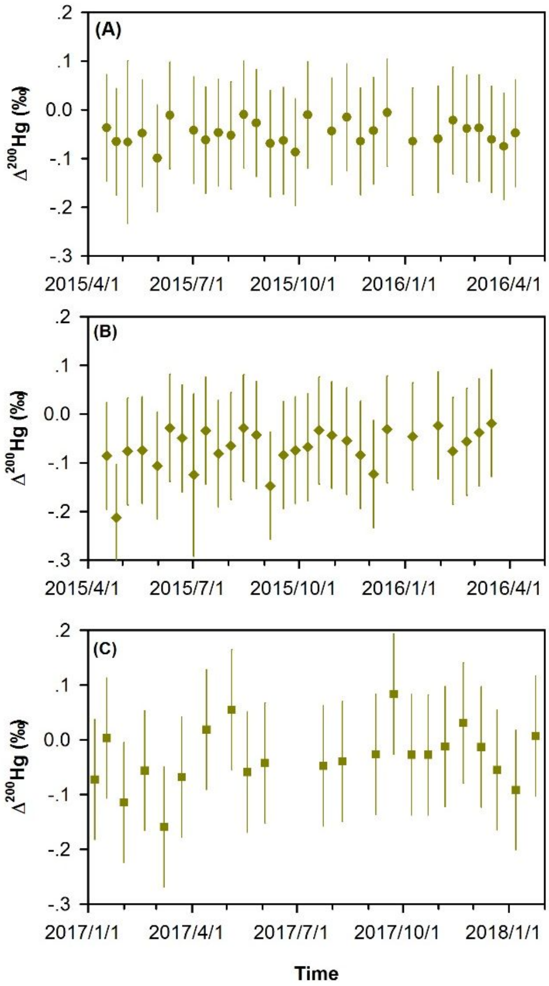

Figure S9. Effects of vegetation activities and mercury emissions on atmospheric TGM $\delta^{202}Hg$. (A-D) TGM $\delta^{202}Hg$ under forest canopy (1 m a.s.l.) in MCB forest versus (A) mean cumulative exposure of 2-d backward trajectories to vegetation NDVI (mean ∑NDVI), (B) mean cumulative exposure of 2-d backward trajectories to anthropogenic Hg^0 emission (mean $\sum Hg^0$ emission), (C) mean cumulative exposure of 2-d backward trajectories to forest fire (mean ∑fire), and (D) fractional air mass residence time over ocean (Fractional oceanic ARTs). (E-H) TGM $\delta^{202}Hg$ above forest canopy (25 m a.s.l.) in MCB forest versus (E) mean ∑NDVI, (F) mean $\sum Hg^0$ emission, (G) mean ∑fire, and (H) Fractional oceanic ARTs. (I-L) TGM $\delta^{202}Hg$ under forest canopy (1 m a.s.l.) in MAL forest versus (I) mean ∑NDVI, (J) mean $\sum Hg^0$ emission, (K) mean ∑fire, and (L) Fractional oceanic ARTs.

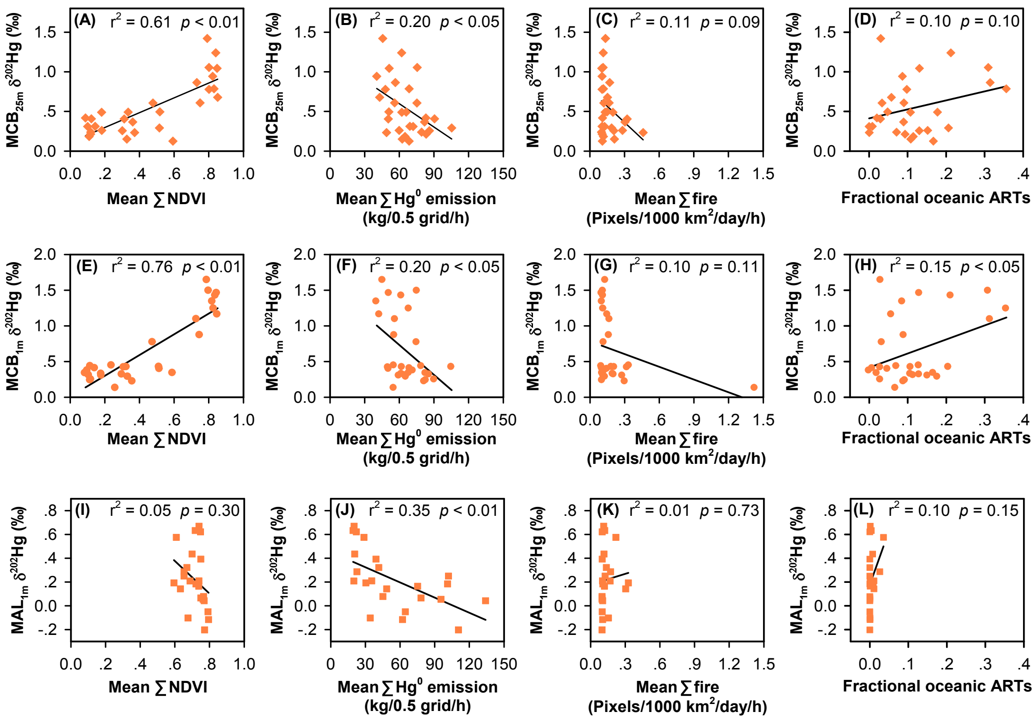

Figure S10. Effects of vegetation activities and mercury emissions on atmospheric TGM Δ^{199}Hg. (A-D) TGM Δ^{199}Hg under forest canopy (1 m a.s.l.) in MCB forest versus (A) mean cumulative exposure of 2-d backward trajectories to vegetation NDVI (mean ∑NDVI), (B) mean cumulative exposure of 2-d backward trajectories to anthropogenic Hg^0 emission (mean ∑Hg^0 emission), (C) mean cumulative exposure of 2-d backward trajectories to forest fire (mean ∑fire), and (D) fractional air mass residence time over ocean (Fractional oceanic ARTs). (E-H) TGM Δ^{199}Hg above forest canopy (25 m a.s.l.) in MCB forest versus (E) mean ∑NDVI, (F) mean ∑Hg^0 emission, (G) mean ∑fire, and (H) Fractional oceanic ARTs. (I-L) TGM Δ^{199}Hg under forest canopy (1 m a.s.l.) in MAL forest versus (I) mean ∑NDVI, (J) mean ∑Hg^0 emission, (K) mean ∑fire, and (L) Fractional oceanic ARTs.

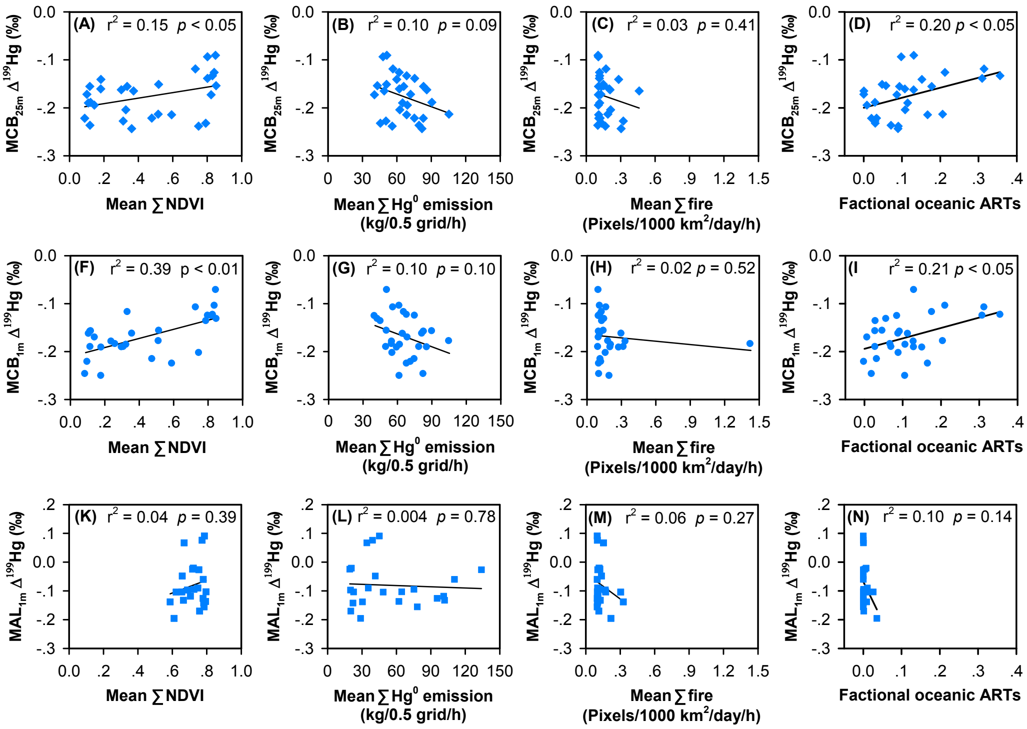

Figure S11 Origins of air masses in MCB forest during the study period. The contour indicates the number of trajectory segment endpoints in a 1°×1° grid cell.

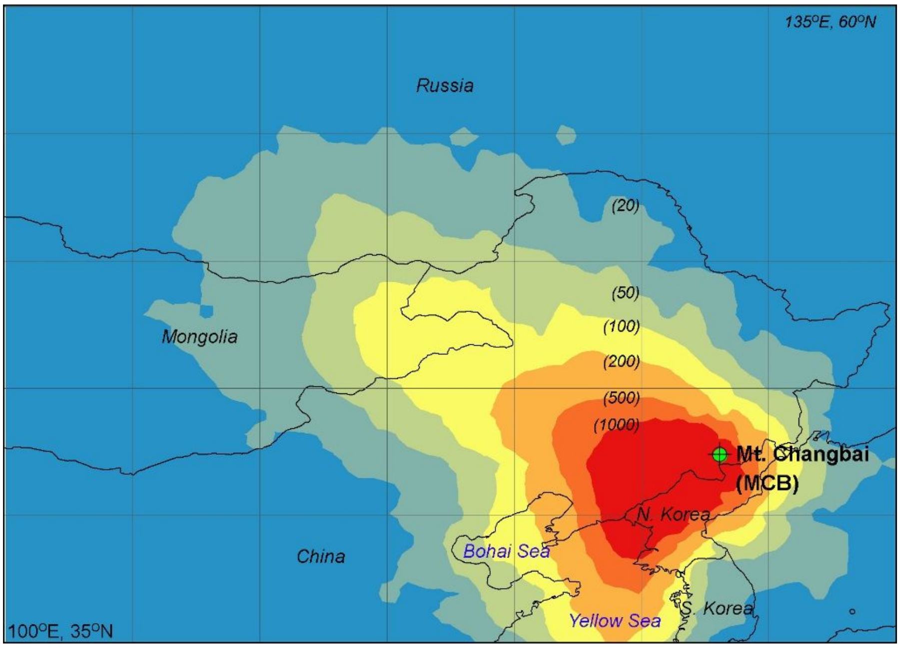

Figure S12 Effect of anthropogenic emissions and vegetation activity on the variations of TGM $\delta^{202}Hg$ and $\Delta^{199}Hg$ in the Northern Hemisphere. (A) means of $\delta^{202}Hg_{TGM}$ at worldwide sites versus means of $\sum Hg^0$ emission at the sites, (B) means of $\delta^{202}Hg_{TGM}$ at worldwide sites versus means of local NDVI at the sites, (C) means of $\Delta^{199}Hg_{TGM}$ at worldwide sites versus means of $\sum Hg^0$ emission at the sites, and (D) means of $\Delta^{199}Hg_{TGM}$ at worldwide sites versus means of local NDVI at the sites. Means of $\sum Hg^0$ emission and NDVI at the worldwide sites were calculated during the sampling period of TGM isotope. 48-h backward trajectories arriving six times daily (00:00, 04:00, 08:00, 12:00, 16:00, and 20:00) at an arrival height of 100 m above ground level were used to determine the means of $\sum Hg^0$ emission at all the sites. means of TGM $\delta^{202}Hg$ and $\Delta^{199}Hg$ at worldwide sites are from this study and the literatures [*Gratz et al.*, 2010; *Demers et al.*, 2013; *Demers et al.*, 2015; *Enrico et al.*, 2016; *Fu et al.*, 2016; *Yu et al.*, 2016; *Obrist et al.*, 2017; *Xu et al.*, 2017; *Fu et al.*, 2018].

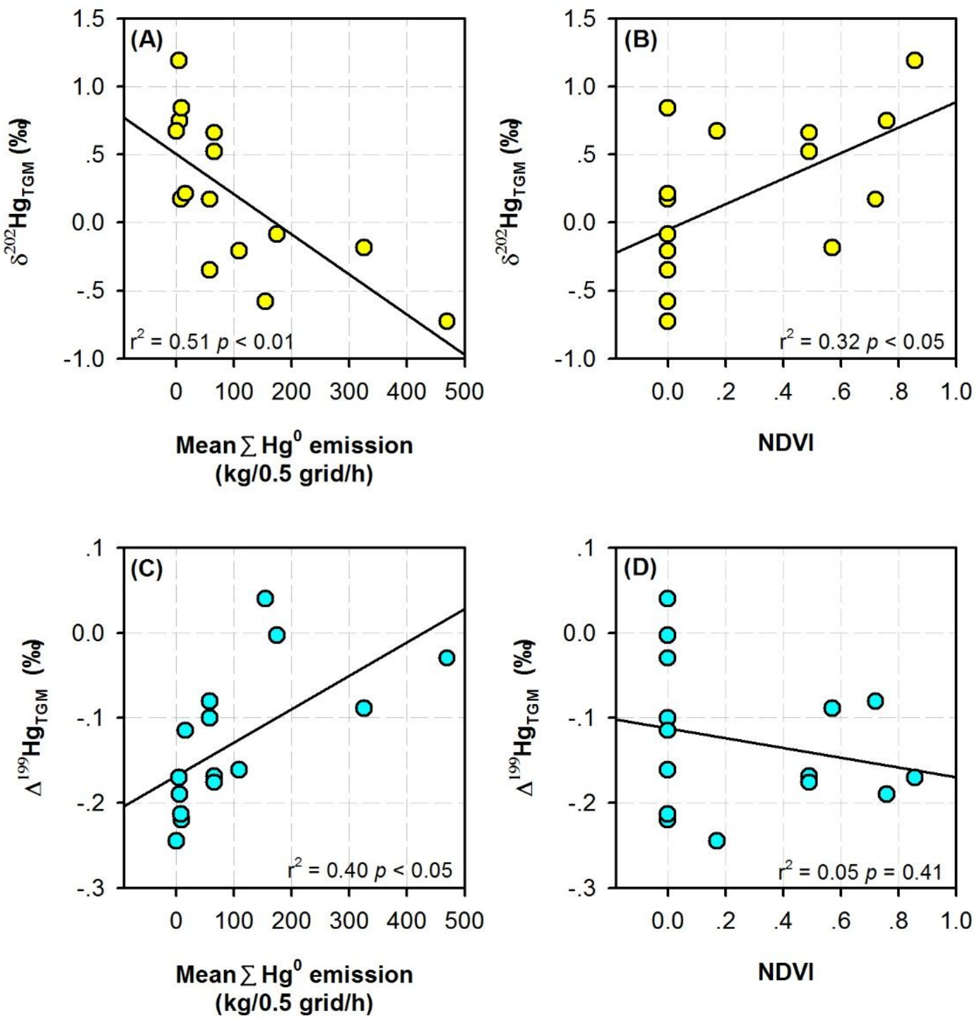

Figure S13 Scatter plot of the measured TGM δ^{202}Hg values versus the predicted TGM δ^{202}Hg values using the means of cumulative anthropogenic Hg^0 emission ($\sum Hg^0$ emission) and the means of local NDVI at worldwide sites. Means of TGM δ^{202}Hg values at worldwide sites are from this study and the literatures [*Gratz et al.*, 2010; *Demers et al.*, 2013; *Demers et al.*, 2015; *Enrico et al.*, 2016; *Fu et al.*, 2016; *Yu et al.*, 2016; *Obrist et al.*, 2017; *Xu et al.*, 2017; *Fu et al.*, 2018].

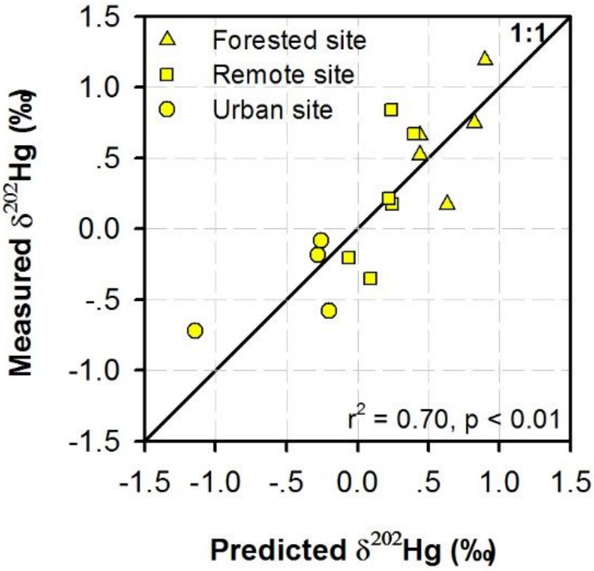

References:

Demers, J. D., J. D. Blum, and D. R. Zak (2013), Mercury isotopes in a forested ecosystem: Implications for air-surface exchange dynamics and the global mercury cycle, *Global Biogeochem Cy*, *27*(1), 222-238.

Demers, J. D., L. S. Sherman, J. D. Blum, F. J. Marsik, and J. T. Dvonch (2015), Coupling atmospheric mercury isotope ratios and meteorology to identify sources of mercury impacting a coastal urban-industrial region near Pensacola, Florida, USA, *Global Biogeochem Cy*, *29*(10), 1689-1705.

Enrico, M., G. Le Roux, N. Marusczak, L. E. Heimburger, A. Claustres, X. W. Fu, R. Y. Sun, and J. E. Sonke (2016), Atmospheric Mercury Transfer to Peat Bogs Dominated by Gaseous Elemental Mercury Dry Deposition, *Environmental Science & Technology*, *50*(5), 2405-2412.

Fu, X., X. Yang, Q. Tan, L. Ming, T. Lin, C.-J. Lin, X. Li, and X. Feng (2018), Isotopic Composition of Gaseous Elemental Mercury in the Marine Boundary Layer of East China Sea, *Journal of Geophysical Research: Atmospheres*, *123*(14), 7656-7669.

Fu, X. W., N. Marusczak, X. Wang, F. Gheusi, and J. E. Sonke (2016), Isotopic Composition of Gaseous Elemental Mercury in the Free Troposphere of the Pic du Midi Observatory, France, *Environmental Science & Technology*, *50*(11), 5641-5650.

Gratz, L. E., G. J. Keeler, J. D. Blum, and L. S. Sherman (2010), Isotopic composition and fractionation of mercury in Great Lakes precipitation and ambient air, *Environmental Science & Technology*, *44*(20), 7764-7770.

Obrist, D., Y. Agnan, M. Jiskra, C. L. Olson, D. P. Colegrove, J. Hueber, C. W. Moore, J. E. Sonke, and D. Helmig (2017), Tundra uptake of atmospheric elemental mercury drives Arctic mercury pollution, *Nature*, *547*(7662), 201-204.

Wang, Y. Q., X. Y. Zhang, and R. R. Draxler (2009), TrajStat: GIS-based software that uses various trajectory statistical analysis methods to identify potential sources from long-term air pollution measurement data, *Environ Modell Softw*, *24*(8), 938-939.

Xu, H., J. E. Sonke, B. Guinot, X. Fu, R. Sun, A. Lanzanova, F. Candaudap, Z. Shen, and J. Cao (2017), Seasonal and Annual Variations in Atmospheric Hg and Pb Isotopes in Xi'an, China, *Environ Sci Technol*, *51*(7), 3759-3766.

Yu, B., et al. (2016), Isotopic Composition of Atmospheric Mercury in China: New Evidence for Sources and Transformation Processes in Air and in Vegetation, *Environmental Science & Technology*, *50*(17), 9262-9269.